Earthquakes and Structures, *Vol. 18, No. 2 (2020) 201-213*
DOI: https://doi.org/10.12989/eas.2020.18.2.201

Seismic effects of epicenter distance of earthquake on 3D damage performance of CG dams

Memduh Karalar[a] and Murat Çavuşli*

Zonguldak Bulent Ecevit University, Department of Civil engineering, Zonguldak, Turkey

(*Received April 25, 2019, Revised November 13, 2019, Accepted November 26, 2019*)

Abstract. Seismic damages that occurred by the effects of epicenter distance of the earthquake are one of the most important problems for the earthquake engineering. In this study, it is aimed to examine the nonlinear seismic behaviors of concrete gravity (CG) dams considering various epicenter distances. For this purpose, Boyabat CG dam that is one of the biggest concrete gravity dams in Turkey is selected as a numerical application. FLAC3D software based on finite difference method is used for modelling and analyzing of the dam. Drucker-Prager nonlinear material model is used for the concrete body and Mohr-Coulomb nonlinear material model is taken into account for the foundation. Special interface elements are used between dam body and foundation to represent interaction condition. Free-field and quiet non-reflecting boundary conditions are utilized for the main surfaces of 3D model. Total 5 various epicenter distances of 1989 Loma Prieta earthquake are considered in 3D earthquake analyses and these distances are 5 km, 11 km, 24 km, 85 km and 93 km, respectively. According to 3D seismic results, *x-y-z* displacements, principal stresses and shear strain failures of the dam are evaluated in detail. It is clearly seen from this study that the nonlinear seismic behaviors of the CG dams change depending to epicenter distance of the earthquake. Thus, it is clearly recommended in this study that when a CG dam is modelled or analyzed, distance of the earthquake fault to the dam should be strongly examined in detail. Otherwise, earthquake damages can be occurred in the concrete dam body by the effects of seismic loads

Keywords: concrete gravity dam; earthquake performance; epicenter distance; interaction condition; non-reflecting boundary condition

1. Introduction

Recently, three dimensional (3D) nonlinear analyzing has obviously become widespread in the civil engineering. This practice has been widely used to assess the earthquake performance of concrete gravity (CG) dams (Wang *et al.* 2017). Nonlinear earthquake behaviors of CG dams under strong seismic loads was investigated by many investigators in the past (e.g., Wang *et al.* 2017, Yazdani and Alembagheri 2017). Firstly, Westergaard has been pioneered to the literature about the seismic modelling and analysis of CG dams. It was suggested very important information about the dam-foundation-reservoir interaction under seismic loads in 1933. In addition, it was examined the importance of the hydrodynamic pressure on rigid dams during earthquakes (Westergaard 1933). In the later years, the effects of water compressibility on the hydrodynamic pressure were examined considering vertical-horizontal ground motions (Chopra 1966). Moreover, the improvements in two dimensional analyses were taken place in the last years of the 20th century (Fenves 1984).

Then, Fok and Chopra studied the seismic flexibility of the dam's foundation considering finite element method (Fok and Chopra 1985). Base of the finite element method in the world was composed by that study.

Hall summarized the results of the dynamic and seismic behaviour of concrete dams taking into account experimental behavior and monitoring evidence (Hall 1988).

Fanelli *et al.* (1992) modelled the dynamic behavior of a concrete dam under strong ground motions and dynamic analyses were performed. According to analysis results, seismic behavior of CG dams was determined and discussed.

Physical modelling of sliding failure of concrete gravity dam under overloading condition was performed. The deformation process and failure mechanism of dam sliding within the rock foundation were investigated based on the test results. It was found that the horizontal displacements at the toe and heel indicate the dam stability condition. During overloading, it was observed that the cracking zone in the foundation can be simplified as a triangle with gradually increased height and vertex angle (Zhu *et al.* 2010).

Effect of non-uniform excitation due to spatially variation of seismic input on nonlinear response of concrete gravity dams was investigated in detail. It was found that tensile damage in neck and toe regions and also, in the vicinity of the base increase when the system is excited non-uniformly (Mirzabozorg *et al.* 2010).

Then, it was examined the ice cover effects on the seismic response of concrete gravity dam reservoir-foundation interaction systems subjected to a horizontal earthquake ground motion. It was observed that the

*Corresponding author, Graduate Research Assistant
E-mail: murat.cavusli@beun.edu.tr
[a]Assistant Professor
E-mail: memduhkaralar@beun.edu.tr

ISSN: 2092-7614 (Print), 2092-7622 (Online)

variations of the length, thickness, and elasticity modulus of the ice-cover influence the displacements and stresses of the coupled system considerably. (Haciefendioglu *et al.* 2010).

Lei (2010) examined the seismic role of reservoir water on the dams considering M=8 Wenchuan earthquake. According to numerical results, reservoir water loads have very important seismic role on the dynamic behavior of the dams.

Chen and DU (2011) investigated elasto-plastic dynamic analysis of a high concrete gravity dam. The dynamic strength reduction method was employed to analyze the anti-sliding stability of the dam under dynamic loads.

Besides, a technique was proposed for dynamic analysis of concrete dam-reservoir systems. Based on this investigation, it was concluded that this approach can be envisaged as a great substitute for the rigorous type of analysis (Lotfi and Samii 2012).

A coaxial rotating smeared crack model was proposed for mass concrete in three-dimensional space. The model is capable of applying both the constant and variable shear transfer coefficients in the cracking process. The model was utilized on Koyna Dam using finite element technique. The results were extracted at crest displacement and crack profile within the dam body. The results showed the importance of both shear transfer coefficient and the fracture energy in seismic analysis of concrete dams under high hydrostatic pressure (Hariri-Ardebili *et al.* 2013).

Frequency domain methods that rigorously incorporate dam-reservoir-foundation interaction and time domain methods with approximate hydrodynamic foundation interaction effects were employed. The maximum principal tensile stresses and their distribution at the dam base, which are important parameters for concrete dam design, were obtained using the frequency domain approach. Prediction equations were proposed for these stresses and their distribution at the dam base. A new effective damping prediction equation was proposed in order to estimate earthquake stresses accurately with the approximate time domain approach (Akpinar *et al.* 2014).

The nonlinear dynamic analysis of Koyna dam was performed using the concrete model with isotropic damage in local approach. Severe damage was found in the form of horizontal cracking observed on both the upstream face of the upper part of dam monoliths (Oudni and Bouafia 2015). In addition, static, modal and transient analyses of dam-reservoir-foundation system were performed using a finite element software. An expression for the fundamental period of concrete dams was developed based on modal analysis (Varughese and Nikithan 2016).

Then, it was presented the effects of geometrical dimensions of concrete gravity dams on the seismic response considering different base width/dam height (L/H) ratios. Finite element models of the dam were constituted including five different L/H ratios such as 0.25, 0.5, 0.75, 1.00, 1.25. The results showed that the L/H ratios considerably affect the seismic response of gravity dams (Sevim 2018).

Seismic performance and failure mode of the Jin'anqiao concrete gravity dam based on incremental dynamic analysis was performed in 2019. It was concluded in that study that under ground motion loadings of the Jin'anqiao dam, the locations at which functional failure may occur are mostly found in the stress concentration of the dam slope, the boundary of the rolling section, the junction between the dam and dam foundation, and the top of the corridor (Chen *et al.* 2019).

Then, the effects of massed layered foundation on seismic response of concrete gravity dams in dam-reservoir-foundation systems were investigated by Sotoudeh. Results showed that how layer properties severely can affect the dynamic responses of the dam (Sotoudeh 2019). In addition, many studies also showed that the dynamic response of concrete dams can be examined by implementation of 2D finite element modelling (Akköse and Şimşek 2010, Zhang and Wang 2013).

As seen these studies, many investigators were examined the seismic behaviour of CG dams. However, the effects of epicenter distance of earthquake on the seismic behavior of CG dams were not observed in the literature. Thus, this study supports many important information to the literature about effects of earthquake's epicenter distance on the nonlinear seismic behaviors of these dams. In this study, Boyabat CG dam has 195 m height is selected for 3D seismic analyses. Dam is modelled using FLAC3D software based on the finite difference method. Drucker-Prager and Mohr-Coulomb nonlinear material models are utilized for concrete body and foundation, respectively. Special interface elements are defined to the discrete surfaces (dam body-foundation). Free field and quiet non-reflecting boundary conditions are used for the main surfaces of 3D model. Earthquake analyses are performed for the full reservoir condition of the dam. Total 5 various epicenter distances of 1989 Loma Prieta earthquake are considered in the nonlinear earthquake analyses. Distances of these ground motions to the center are 5 km, 11 km, 24 km, 85 km and 93 km, respectively. Main aim of this study is to assess the effects of these distances on 3D nonlinear earthquake behavior of Boyabat CG dam. According to analysis results, *x*-*y*-*z* displacements, principal stresses and shear failures of five different nodal points selected on the dam body are evaluated in detail and these results are compared with each other. In this study, it is clearly seen that epicenter distance of earthquake has very critical seismic effects on the 3D earthquake behavior of CG dams. When this distance increases or diminishes, earthquake behavior of the dam clearly changes.

2. Boyabat concrete gravity dam

State Hydraulic Works (DSI) is very important institution in Turkey and it is responsible for planning and implementation of water resources development projects in Turkey. Total 204 large dams and 339 moderate dams were constructed by DSI. Besides to those completed projects, 111 large dams and 159 moderate dams are also under construction. The Boyabat Dam was constructed as a concrete gravity dam by DSI and it is located in the north of Turkey, about 123 km further from the Black Sea border, on the Kızılırmak River, 10 km southwest of the Durağan district center. The project area is surrounded by the IlgazMountains, reaching 1500-1600 m elevations in the

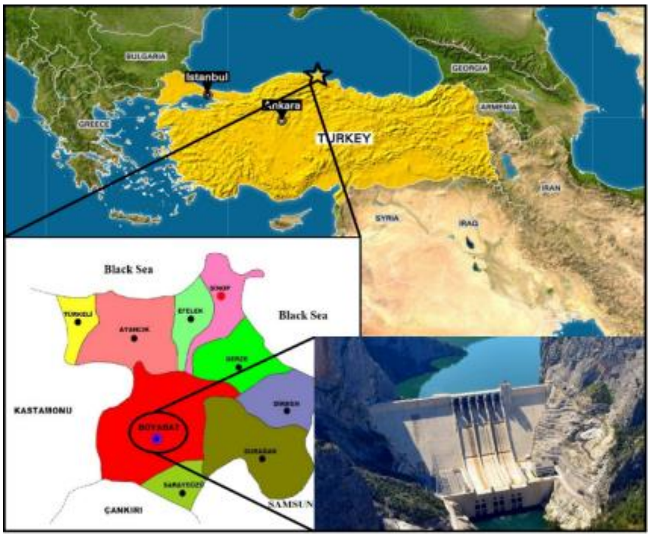

Fig. 1 Location and general view of Boyabat dam

Table 1 Material properties of Boyabat CG dam

Material	Modulus of Elasticity (GPa)	Poisson's Ratio	Mass Density (kg/m³)
Concrete (Dam)	30	0.20	2530
Rock (Foundation Soil)	25	0.18	2800

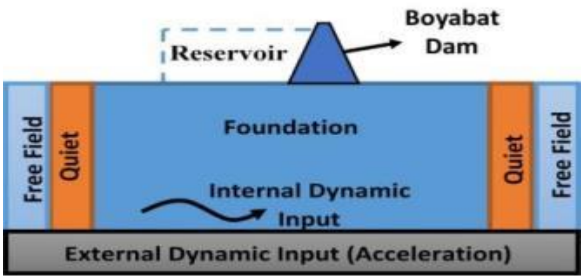

Fig. 2 Quiet seismic boundary condition in the finite difference models

north and west (Fig. 1). It is also surrounded by Kunduz and Ç al Mountains in the south and Altinkaya Dam Reservoir in its downstream. The dam site is 120 km west of the province of Samsun and 80 km south of Sinop province. The Boyabat dam was completed in 48 months and energy production was started on 5 November 2012. Boyabat dam's height is 195 m and maximum water level is 190 m. Elevation of dam crest is 335.00 m. Dam body volume is 2300000 m^3. The total lake volume is 3557000000 m^3. In addition, drainage area is 64724 km^2. There is 6 spillway cover in the dam. The spillway capacity is 9300 m^3/s. Material properties of Boyabat concrete gravity dam is shown in Table 1 in detail. According to Table 1, modulus of elasticity of concrete dam body is 30 GPa and this numerical value is 25 GPa for the foundation. Moreover, poisson's ratio of concrete body is 0.20 and it is 0.18 for the foundation. Finally, mass density is 2530 kg/m^3 and 2800 kg/m^3 for concrete body and foundation, respectively. These material properties are obtained from the original dam project and these parameters are defined to 3D finite difference model of the dam using special fish functions.

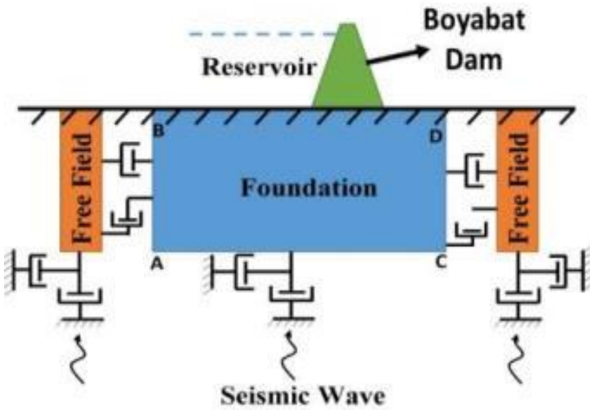

Fig. 3 View of free field seismic boundary condition in the 3D model

3. Calculation theory

3.1 Quiet (viscous) boundary condition

While analyzing special structures such as dams, many seismic boundary conditions were used for the lateral and bottom surfaces of the 3D model in the past. However, many of these seismic boundary conditions are reflecting seismic boundaries. Reflecting boundary condition (fix boundary condition) does not provide true numerical results for the dynamic analyses. Because the fix boundary condition does not represent reality. In the static analyses, fix or elastic boundary condition can be used for the main surfaces of 3D model of the dam. However, this reflecting boundary condition brings about reflecting earthquake waves back to the 3D model and this numerical process does not transfer the necessary seismic energy. For this reason, non-reflecting boundary conditions should be used for seismic analyses of concrete gravity dams. Quiet (viscous) boundary condition is an alternative non-reflecting boundary condition for seismic analyses. This viscous boundary was developed by Lysmer and Kuhlemeyer (Lysmer and Kuhlemeyer 1969). In this alternative condition, the seismic dashpots for normal and shear directions of special boundaries of the 3D model are used. Moreover, this boundary condition is very effective for absorbing earthquake loads that approached to the surface at angle greater than 30°. In this study, the quiet (viscous) boundary condition is practiced to lateral boundaries of the 3D model as seen in Fig. 2.

This special seismic boundary condition takes into account the seismic dashpots that were defined to the boundaries of the 3D model in the normal and shear directions. Thus, viscous normal and shear tractions are provided and these tractions can be defined as Eq. (1).

$$\begin{aligned} t_n &= -\rho C_p v_n \\ t_s &= -\rho C_s v_s \end{aligned} \tag{1}$$

where: V_n is normal shear component, V_s is shear component, C_p is p wave velocity, C_s is s wave velocity and ρ is the density.

3.2 Free field seismic boundary condition

Free field boundary is a special boundary condition for seismic analyses of water structures. In this study, free field boundary condition is defined to the lateral surfaces of the 3D model using special fish functions. Free field boundary condition in the 3D model of Boyabat CG dam is presented in Fig. 3.

The lateral surfaces of the 3D finite difference model are merged to the free field surfaces with viscous dashpots (quiet seismic boundary condition). This seismic condition is expressed in Eq. (2).

$$F_x = -\left[\rho C_p \left(v_x^m - v_x^{ff}\right) - \sigma_{xx}^{ff}\right]\Delta S_y$$
$$F_y = -\left[\rho C_s \left(v_y^m - v_y^{ff}\right) - \sigma_{xy}^{ff}\right]\Delta S_y \qquad (2)$$

ρ = density along vertical surface,
C_p = speed of *p*-wave at the left surfaces of the 3D model,
C_s = speed of *s*-wave at the left surfaces of the 3D model,
Δ_{sy} = vertical zone size at boundary gridpoint,
v_m^x = *x*-velocity for gridpoint at left surfaces,
v_y^m = *y*-velocity for gridpoint at left surfaces,
σ_{xx}^{ff} = mean horizontal free-field stress of gridpoint,
v_x^{ff} = *x*-velocity for gridpoint in left free field,
v_y^{ff} = *y*-velocity for gridpoint in left free field and

In this seismic boundary condition, earthquake waves that propagates upward do not break down at the main surfaces. If grid point is uniform, the seismic dashpots are not considered due to the free field surface performs the same motion as the main grid. However, when the grid motion differentiates from the free field boundary condition, the seismic dashpots behave close to the quiet boundaries for absorbing earthquake loads. The free-field boundary condition model contains one-dimensional column at unit width. The free field's height equals the lateral surface's length (Itasca 2002).

In this study, hysteretic damping sigmoidal (sig3) model was used for the damping ratios of foundation and concrete. The dynamic characteristics of these materials were governed by two sets of modulus reduction factor (G/G_{max}) of the foundation and concrete and damping ratio (λ). Hysteretic damping equation is shown in Eq. (3).

$$Ms = \frac{a}{1 + \exp(-(L - x_0)/b)} \qquad (3)$$

First in literature, numerical fits for sig3 model (a, b, x_0, L) were determined for sand by Seed and Idriss (1972) and these fits were calculated as a=1.014, b=-0.4792, x_0=-1.249. In this study, these fits (a, b, x_0, L) were calculated according to G/G_{max} ratio of material.

4. Geologic background and ground motion inputs

Turkey is located in one of the most actively deforming regions in the world. The tectonic in Turkey depends on relative motions among the African, the Aegean, the the Anatolian, the Black Sea and the Eurasian plates. The

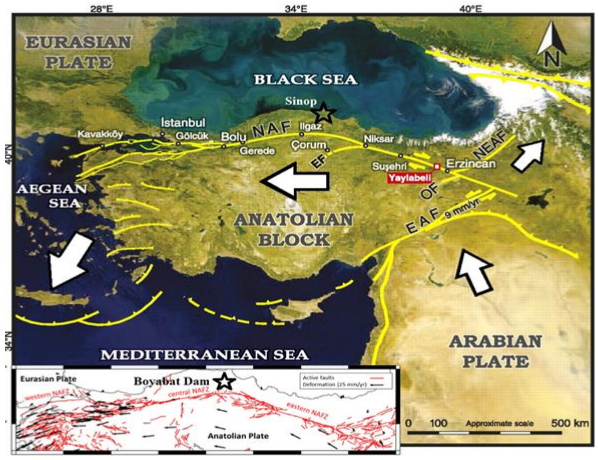

Fig. 4 Fault map of Turkey

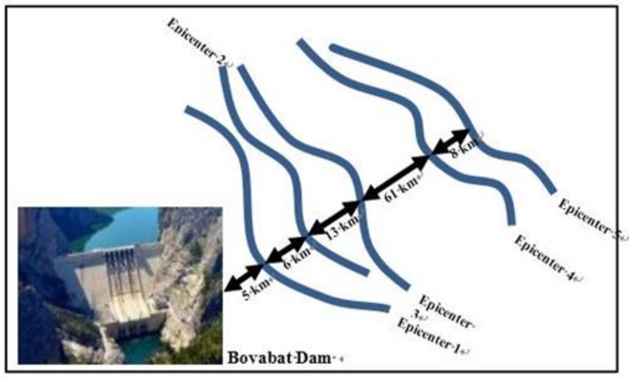

Fig. 5 Various epicenter distances of 1989 Loma Prieta earthquake

neo-tectonics of Turkey is directed by three major elements: a) The Aegean–Cyprean Arc, a convergent plate boundary where the African Plate to the south is sub ducting beneath the Anatolian Plate to the north; b) The North Anatolian Fault (NAF) Zone; c) The East Anatolian Fault (EAF) Zone. The Boyabat dam was built very close to the North Anatolian Fault (NAF). NAF is one of the largest currently active continental strike-slip faults in the world and it extends along more than 1200 km from the Karliova triple junction in the east to the northern Aegean in the west (Fig. 4).

NAF is one of the best-studied strike-slip fault zones on Earth now. The fault developed in relation with the Arabian Plate in the east and the Hellenic subduction zone in the west. Due to its long and extensive historical record of the large earthquakes, the NAF zone provides an important natural laboratory to understand earthquake mechanics and fault behaviour over multiple earthquake cycles. Although the long historical record of the region, all historical earthquakes records for the North Anatolian Fault zone is not yet available. For many centuries, there have been large-magnitude (M>7) earthquakes in the NAF zone. Of these, the most extreme is the İzmit (Mw 7.4) and Düzce (Mw 7.1) earthquakes of 1999.

In this study, 5 various ground motions of 1989 Loma Prieta earthquake are used in the 3D nonlinear earthquake analyses of Boyabat CG dam. These ground motions are

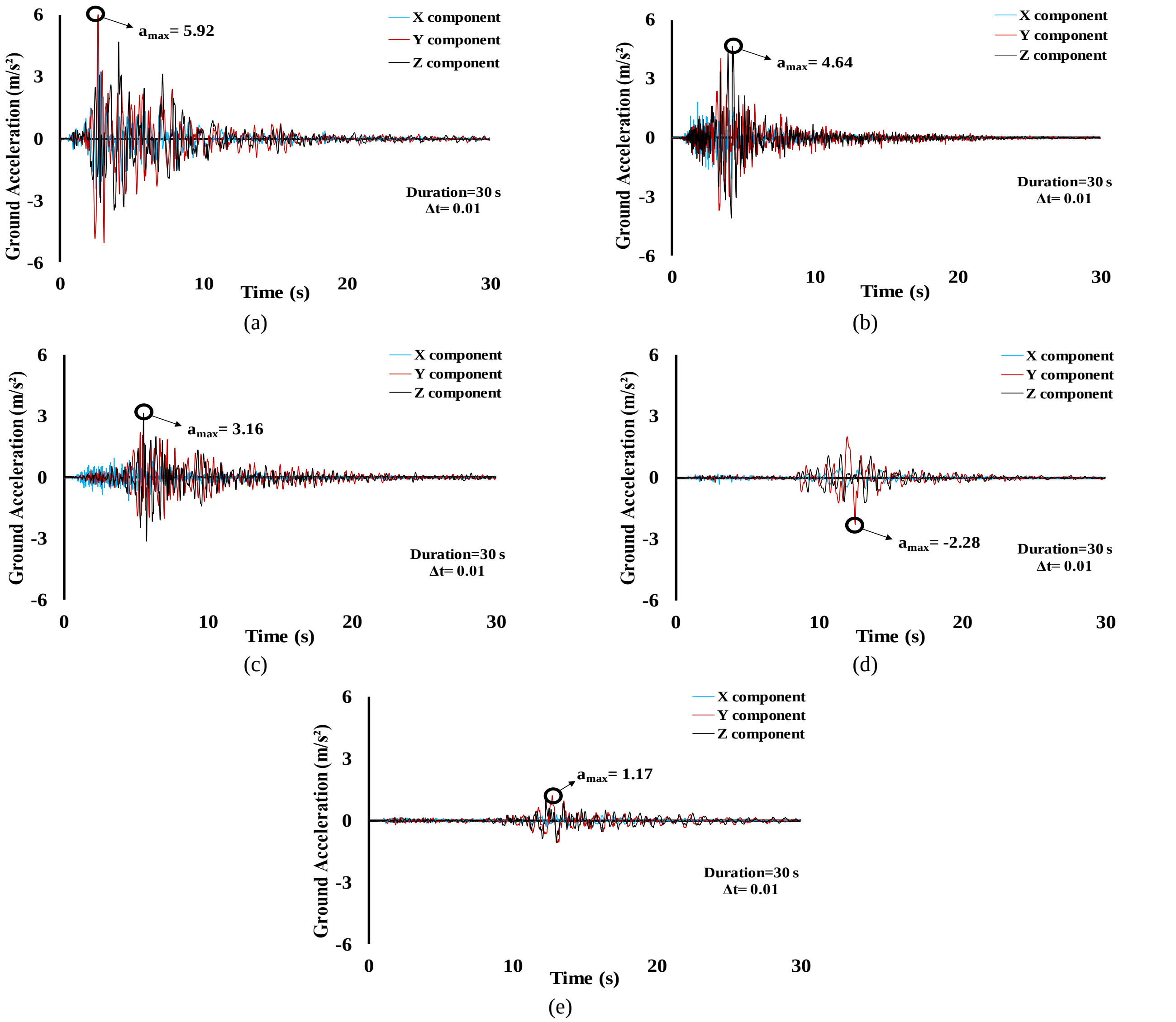

Fig. 6 Time history graphics for (a) Case 1 (Epicenter Distance: 5 km), (b) Case 2 (Epicenter Distance: 11 km), (c) Case3 (Epicenter Distance: 24 km), (d) Case 4 (Epicenter Distance: 85 km), (e) Case 5 (Epicenter Distance: 93 km)

Table 2 Characteristic properties of each ground motion

Case	Case 1	Case 2	Case 3	Case 4	Case 5
Epicenter Distance	5 km	11 km	24 km	85 km	93 km
Station	Corralitos	Gilroy Array	Gilroy Array	Golden Gate	Richmond City
HP (Hz)	0.2	0.2	0.2	0.2	0.2
LP (Hz)	50.0	48	40	30	25
PGA (g)	0.644	0.473	0.323	0.233	0.124
PGV (cm/s)	55.2	33.9	16.6	11.3	4.4
PGD (cm)	11.37	8.03	3.26	2.92	1.27

measured from various distances (Fig. 5). According to Fig. 5, distance of epicenter 1 to the center is 5 km. This ground motion is near fault and it has very significant accelerations. Distance of epicenter 2 to the center and epicenter 3 to the center is 11 km and 23 km, respectively.

Moreover, this distance is 85 km and 93 km for epicenter 4 and epicenter 5, respectively. Epicenter 5 has lower accelerations as compared with others. In Table 2, characteristic properties (HP, LP, PGA, PGV and PGD) of these ground motions are presented in detail. Moreover, time-acceleration graphics of these ground motions are shown in Fig. 6.

5. 3D modelling and calibrating of Boyabat concrete gravity dam

3D modelling and investigating of the seismic behaviors of concrete gravity (CG) dams such as Boyabat CG dam is vital importance to evaluate the future and safety of such dams. In this section, important information about the modelling of Boyabat dam are explained in detail. Because of Boyabat dam is one of the biggest water structures in Turkey, examining and modelling seismicity of this dam provides significant contributions to the literature. Firstly, the foundation of 3D finite difference model is modelled

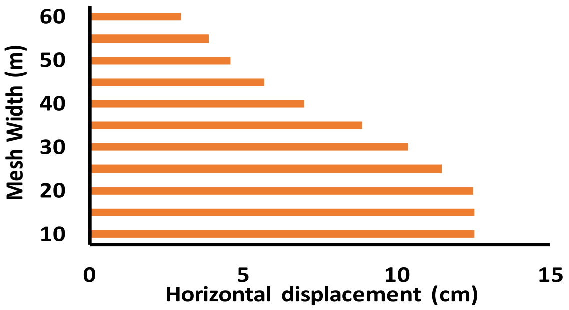

Fig. 7 Horizontal displacement changes on the crest for different mesh widths

taking into account the geological structure of the canyon.While modelling the foundation, the height of the foundation is considered as the height of the dam body. Moreover, the foundation is extended towards the dam body's right and left directions as the height of the dam body. While creating the geometry of the dam body, 3D model of all materials is modelled in accordance with the original dam project. In addition, the height of the dam body is modelled in accordance with the elevation of the rough terrain. Totally, there are 2651998 nodal points in the 3D model of Boyabat Dam. Mesh ranges are not randomly created in the 3D model. The most stable mesh range is taken into account in this study as seen in Fig. 7. In order to find correct mesh width, total of 11 different mesh widths were created and seismic analyses were performed for various mesh width. These widths are 10 m, 15 m, 20 m, 25 m, 30 m, 35 m, 40 m, 45 m, 50 m, 55 m, and 60 m, respectively. It is seen from numerical analyses that the maximum horizontal displacements on the crest of the dam do not change for less mesh width than 20 m (Fig. 7). Thus, mesh width is selected approximately 20 m for seismic analyses.

After the solid model was divided into small pieces (meshing), transverse joint length is chosen as an equal to the mesh length as automatically in FLAC3D. Moreover, in this study, special interface elements are used between the dam body-foundation and dam body-reservoir water to represent the interaction condition of discrete surfaces (Fig. 8). Normal (k_n) and shear (k_s) interaction stiffness values are different for each interface surface. Unit of the k_n and k_s stiffness is stress/displacement (Itasca 2002). In this study, k_n and k_s stiffness are separately calculated for each discrete surface. These stiffness values are considered as approximately 10^8 Pa/m between the dam body and foundation. Shear and normal stiffness values are defined to FLAC3D software using special fish functions. The reservoir water is modelled considering the hydrostatic pressure and leakage in the dam body taking into account the maximum water height (195 m). Free field and quiet (viscous) boundary conditions are applied only lateral surfaces of the 3D model. Firstly, free field special seismic boundary condition is defined to software using special fish functions. Afterwards, the quiet boundary condition is considered to lateral surfaces of the 3D model (Fig. 8). Total 5 various ground motions are used in this study. These earthquakes are practiced to the main surface of the dam.

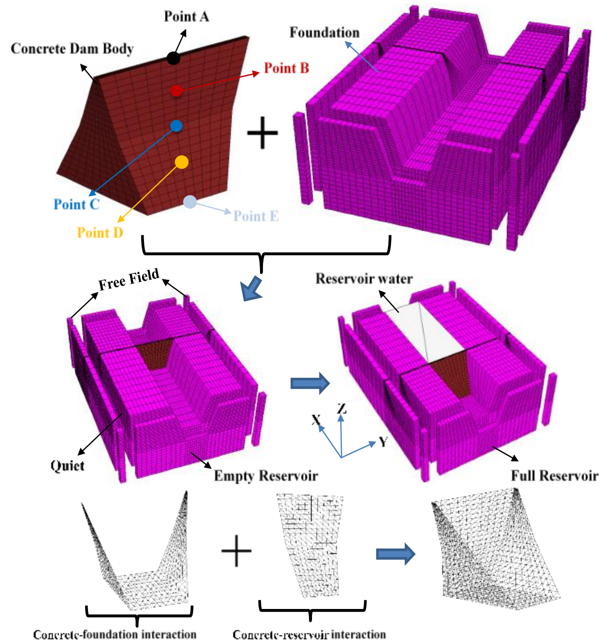

Fig. 8 Three dimensional finite difference model of Boyabat CG dam

6. Three dimensional finite difference analysis results

When examined the literature, it is clearly seen that there are no many studies related with the effects of different epicenter distances of the earthquake on the nonlinear seismic behaviour of concrete gravity (CG) dams. In order to fill these deficiencies, the nonlinear seismic behaviour of Boyabat CG dam is examined considering 5 various epicenter distances of earthquake (5 km, 11 km, 24 km, 85 km and 93 km) in this study. Each distances are represented as a case in this study and these cases are shown in Table 2. Five different nodal points are selected on the dam body surface to better seen changing of nonlinear seismic behavior of Boyabat CG dam. These nodal points are presented in Fig. 8 in detail. As a result of the seismic analyses, principal stresses, shear strain rates, horizontal displacements (x and y directions), and vertical displacements (z direction) are presented and assessed graphically for these nodal points. In addition, these numerical results are compared with each other. Numerical analyses results are presented in Figs. 9-13 in detail. In Fig. 9(a), x displacement results are shown for Case 1. According to Fig. 9(a), maximum x displacement is observed on Point *A* (crest point) and its numerical value is +19.7 cm. Moreover, minimum displacement occurred on Point *E* (the lowest nodal point). During first 3 seconds, there are no significant displacement values on the dam body surface and very critical x displacement values for concrete gravity dams occurred after 3^{th} second of the earthquake. However, very different displacement results are obtained for Case 2 in Fig. 9(b). When examined Fig. 9(b), it is clearly seen the effects of epicenter distance on the nonlinear seismic behavior of Boyabat CG dam. Maximum x displacement occurred on the crest point

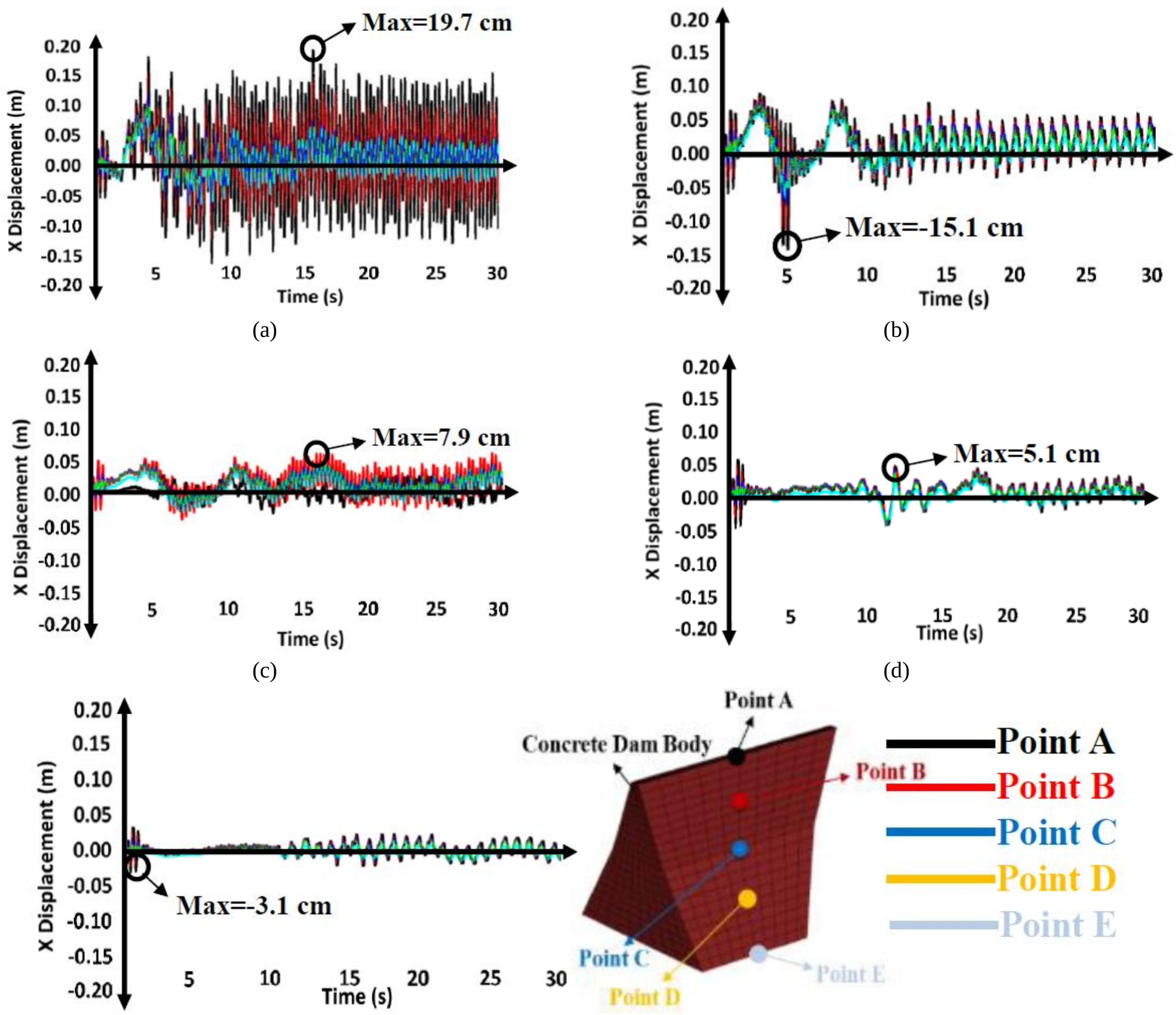

(e)

Fig. 9 Horizontal displacement (*X* direction) results for (a) Case 1 (epicenter distance: 5 km) (b) Case 2 (epicenter distance: 11 km) (c) Case 3 (epicenter distance: 24 km) (d) Case 4 (epicenter distance: 85 km) (e) Case 5 (epicenter distance: 93 km

of the dam body. Its numerical value is -15.1 cm and this maximum displacement is observed at 5th second of the earthquake. As compared Figs. 9(a) and 9(b), it is clearly understood that when the distance of epicenter to the dam increases, maximum *x* displacements progressively diminish. In addition, it is obviously seen that although maximum displacement is positive direction for Case 1, maximum displacement is observed as negative direction for Case 2. In Fig. 9(c), *x* displacement results are shown for Case 3. According to Fig. 9(c), maximum displacement (+7.9 cm) occurred on Point *B* and minimum *x* displacement is observed on Point E. Although maximum displacement is obtained on Point A (crest point) for Cases 1 and 2, maximum *x* displacement occurred on Point B for Case 3. According to Fig. 9(d), maximum displacement for Case 4 is observed on Point *A* and its numerical value is 5.1 cm. No significant *x* displacements are observed for all nodal points during first 7 seconds. Maximum displacement occurred at 12.3th second of the earthquake. Finally, *x* displacement results are shown for Case 5 in Fig. 9(e). According to Fig. 9(e), very small *x* displacements are observed during earthquake duration. Maximum *x* displacement occurred on Point A and this displacement value is -3.1 cm. The effects of epicenter distance on 3D earthquake behavior of CG dams are clearly determined with these numerical results. When compared Cases 1-5, maximum *x* displacement occurred in Case 1 and minimum displacement is observed in Case 5. In addition, *x* displacements on the dam body surface clearly diminish as the epicenter distance increases from 5 km to 24 km. However, when this distance increases from 24 km to 93 km, there are no large displacement changes on the dam body. These results give very important information to the researchers about modeling and construction of concrete gravity dams. Moreover, maximum *x* displacements for all cases are shown in Table 3. In Fig 10, *y* displacement results are graphically shown under 5 various epicenter distances. 5 different nodal points are selected from dam body surface and *y* displacements for these nodal points are compared in the graphics. In Fig. 10(a), displacements are examined for

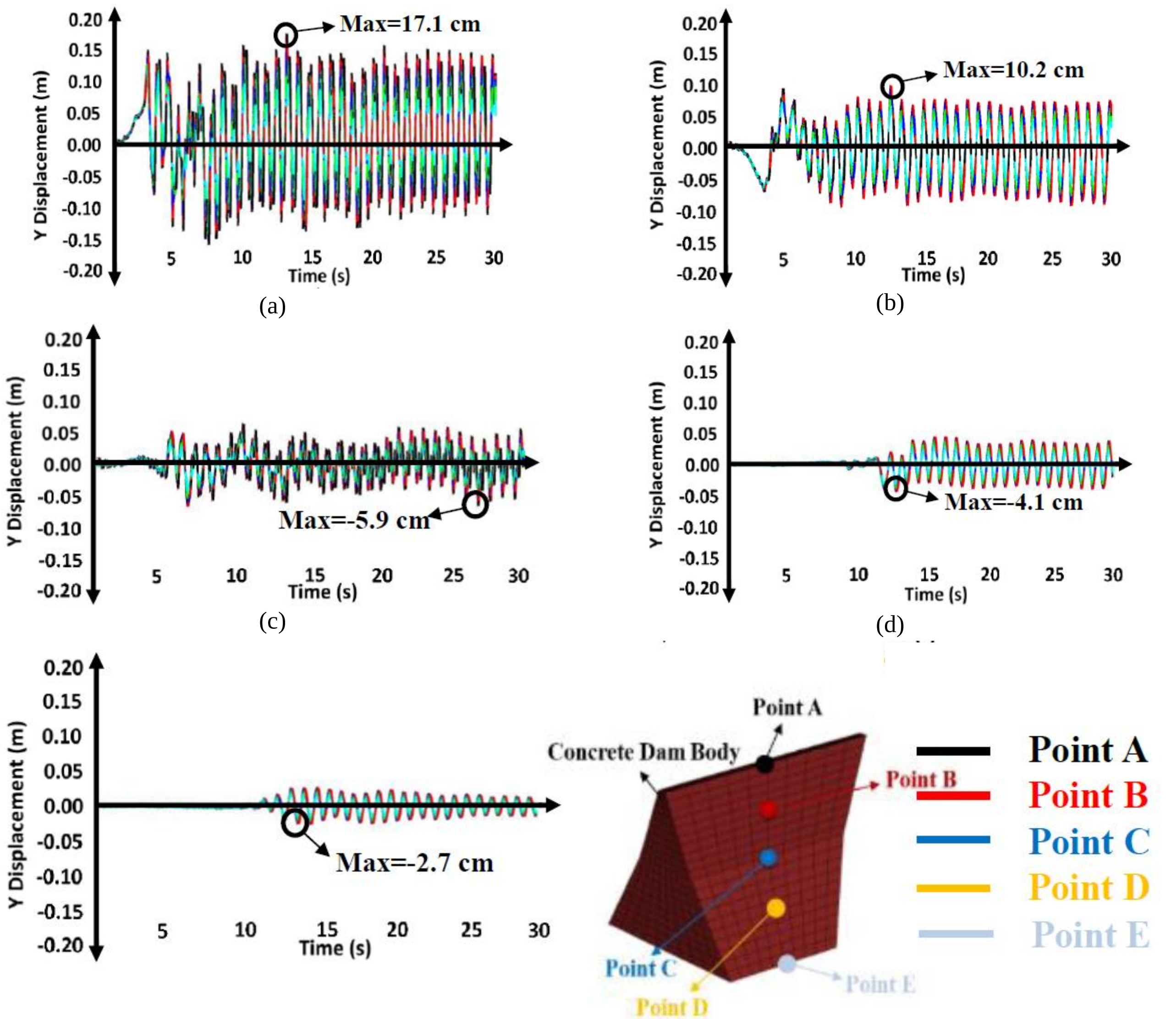

(e)

Fig. 10 Horizontal displacement (*Y* direction) results for (a) Case 1 (epicenter distance: 5 km) (b) Case 2 (epicenter distance: 11 km) (c) Case 3 (epicenter distance: 24 km) (d) Case 4 (epicenter distance: 85 km) (e) Case 5 (epicenter distance: 93 km)

Table 3 Maximum *x* displacements for all case

	Case 1	Case 2	Case 3	Case 4	Case 5
Max. Disp. (cm)	+19.7	-15.1	+7.9	+5.1	-3.1

Table 4 Maximum *y* displacements for all cases

	Case 1	Case 2	Case 3	Case 4	Case 5
Max. Disp. (cm)	+17.1	+10.2	-5.9	-4.1	-2.7

Case 1. According to Fig. 10(a), maximum *y* displacement is +17.1 cm and this numerical value occurred on the crest point of the dam (Point A). Moreover, minimum displacement is observed on Point E. 17.1 cm is very critical displacement value for CG dam's seismic safety. Because 17.1 cm horizontal displacement on the crest point of the dam may cause significant and dangerous concrete cracks in the dam body. Maximum *x* displacements for all cases are presented in Table 4.

In Fig. 10(b), *y* displacements are shown for Case 2 and it is clearly seen that maximum *y* displacement is 10.2 cm. This numerical value is observed on Point *B*. Although maximum displacement occurred on Point *A* for Case 1, maximum displacement for Case 2 is observed on Point B. Moreover, when compared Figs. 10(a) and 10(b), it is obviously seen the effects of epicenter distance on the 3D seismic displacement behavior of CG dams. According to Fig. 10(c), maximum *y* displacement is -5.9 cm and it occurred on the crest point. Crest point (Point A) moved both directions (negative and positive) during the earthquake. This moving may give rise to very important security problems. Thus, as modelled or analyzed a concrete gravity dam, both displacement directions should be examined in detail. Moreover, there are no significant displacements on dam body surface during first 5 seconds of the earthquake for Case 3 as seen Fig. 10(c). In Fig. 10(d), *y* displacement results are shown for Case 4. According to Fig. 10(d), it is clearly seen that maximum *y* displacement is -4.1 cm on the Point B. Very different

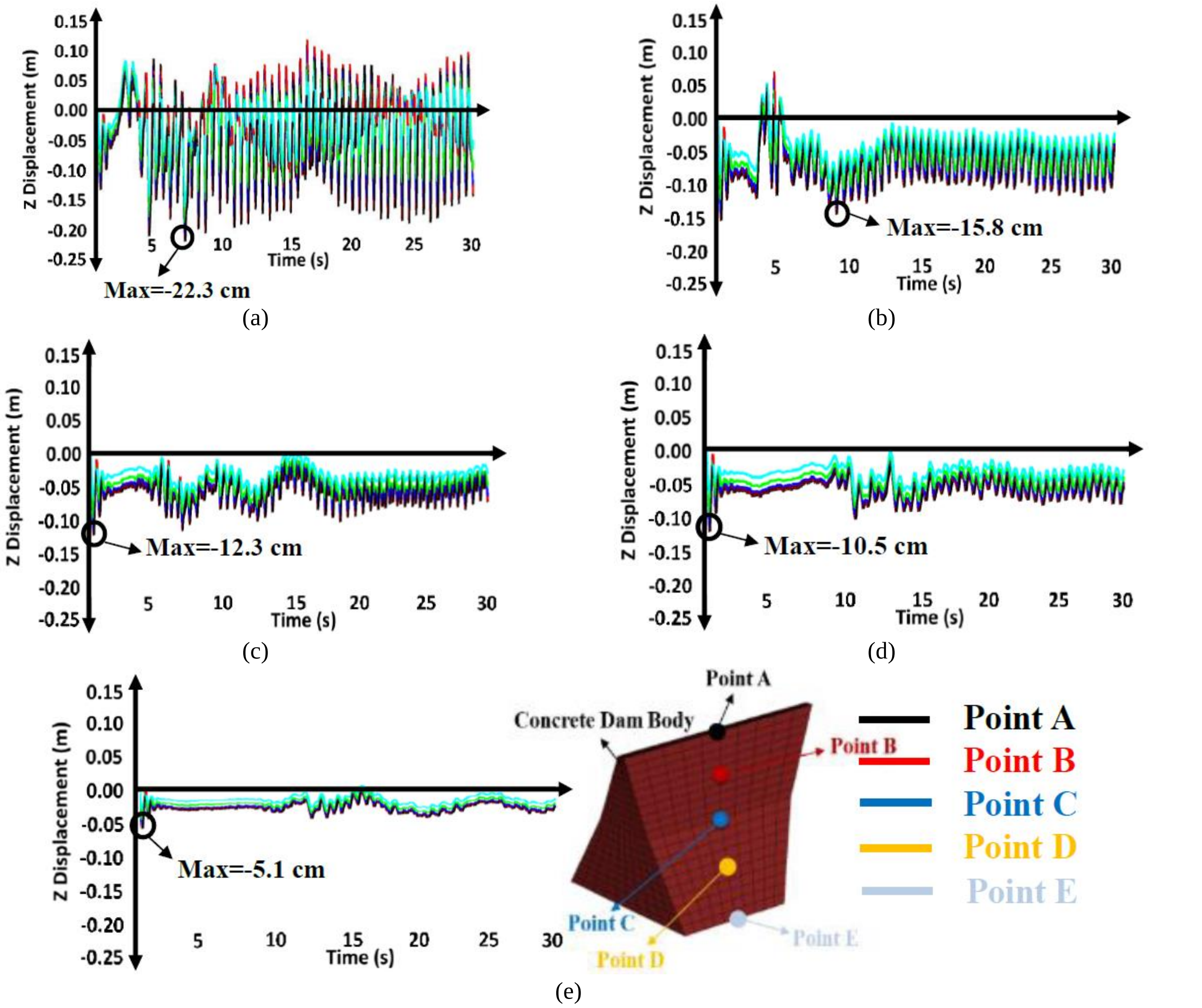

Fig. 11 Vertical displacement (Z direction) results for (a) Case 1 (epicenter distance: 5 km) (b) Case 2 (epicenter distance: 11 km) (c) Case 3 (epicenter distance: 24 km) (d) Case 4 (epicenter distance: 85 km) (e) Case 5 (epicenter distance: 93 km)

displacement results are obtained for Case 4 as compared with other cases. It is obviously seen that very small displacement values occurred during first 10 seconds of the earthquake. It is clearly understood from this important result that when epicenter distance of the earthquake increases, the earthquake loads have less impact on the dam body surface. In Fig. 10(e), *y* displacement results are presented for Case 5. As seen from Fig. 10(e), maximum *y* displacement is -2.7 cm and it occurred on the Point B. During first 13 seconds of the earthquake, there are no significant displacements on the dam body surface. As seen from these numerical results, it is clearly understood that when epicenter distance increases, *y* displacements on the dam body surface clearly diminish. Thus it is clearly recommended in this study that before constructed a concrete gravity dam, epicenter distance should be controlled and analyzed in detail. Otherwise, significant seismic damages can occur on the dam body by effects of the earthquake loads.

In Fig. 11, *z* displacement results for 5 various epicenter distances are shown graphically. It is clearly seen from these numerical results that if a concrete gravity dam is close to the earthquake fault, vertical displacements on the dam body surface are very large depending to the epicenter \distance. In Fig. 11(a), *z* displacement results are shown for Case 1 and maximum displacement is obtained on the Point *A* (crest point). Its numerical value is -22.3 cm and this value is very critical for structural engineering. Sometimes, this displacement value may give rise to cracks on the dam body surface and this situation may cause very critical safety problems for the dam engineering. Moreover, minimum displacement is observed on Point *E* (lowest nodal point). Close displacement results are obtained for Points *A* and *C* for Case 1. This is evidence that different settlements can occur on all surfaces of the dam body during the earthquake. According to Fig. 11(b), displacement results are shown for Case 2. It is clearly seen that maximum *z* displacement occurred on Point *C* and its numerical value is -15.8 cm. When compared Figs. 11(a) and 11(b), it is obviously seen the effects of the epicenter

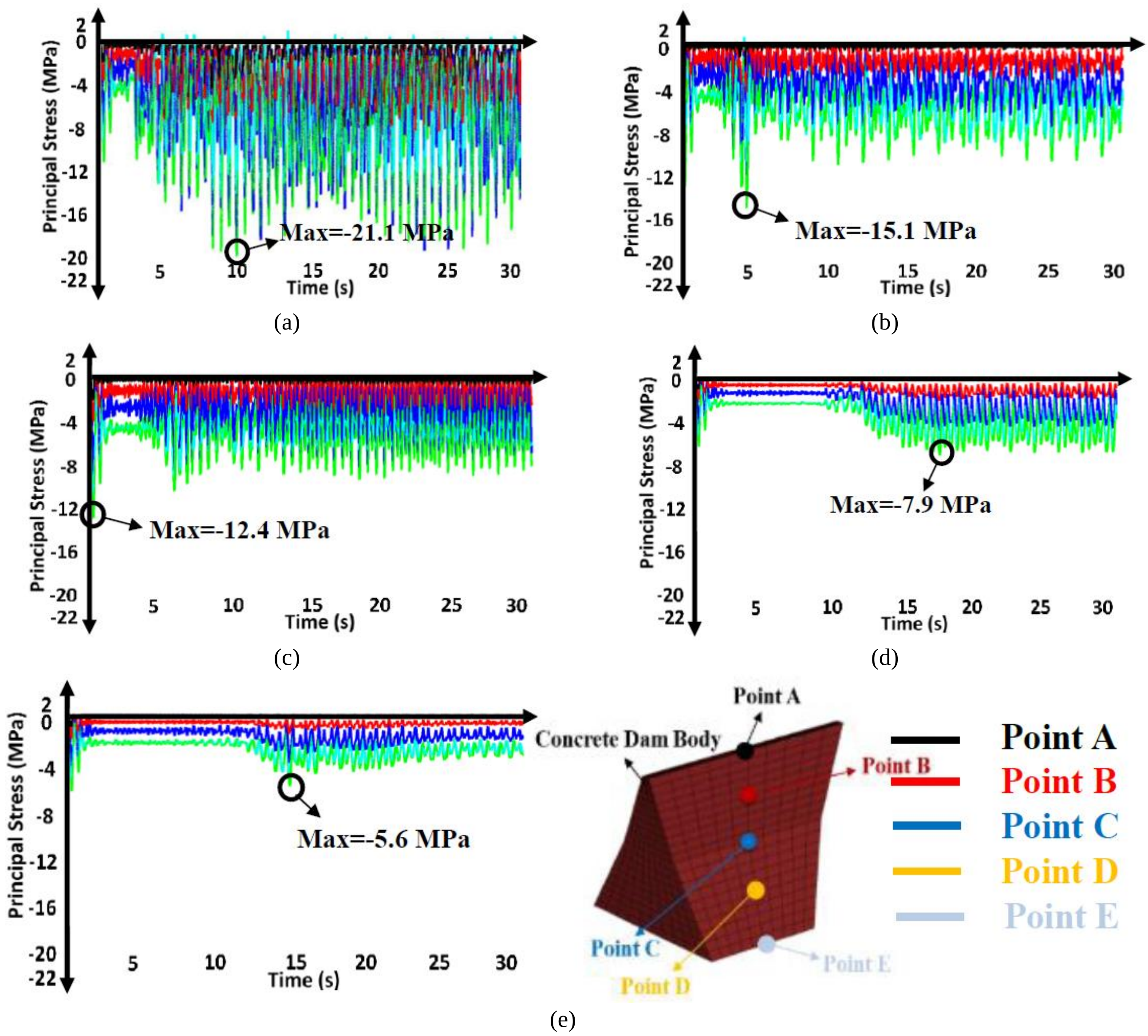

Fig. 12 Principal stress results for different epicenter distances of Loma Prieta earthquake: (a) Case 1 (epicenter distance: 5 km) (b) Case 2 (epicenter distance: 11 km) (c) Case 3 (epicenter distance: 24 km) (d) Case 4 (epicenter distance: 85 km) (e) Case 5 (epicenter distance: 93 km)

Table 5 Maximum *z* displacements for all cases

	Case 1	Case 2	Case 3	Case 4	Case 5
Max. Disp. (cm)	-22.3	-15.8	-12.3	-10.5	-5.1

distance on the 3D nonlinear settlement behavior of the CG dams. Totally, there is 6.5 cm displacement difference between Case 1 and Case 2 and this result is very important for CG dam's seismic performance. In Fig. 11(c), *z* displacement results are presented for Case 3. As seen from Fig. 11(c), maximum *z* displacement is -12.3 on Point *A*. Close displacements are obtained for Points *A* and *C*. Moreover, minimum displacement occurred on Point *E*. According to Fig. 11(d), it is clearly seen that maximum *z* displacement is -10.5 cm and it occurred on the Point *A*. In addition, -10.2 cm *z* displacement is obtained on Point *C*. Finally, *z* displacements are examined for Case 5 in Fig. 11(e). According to Fig. 11(e), maximum settlement value is -5.1 cm and minimum displacements are observed on Point *E*. Very close displacements are acquired on 5 nodal points for Case 5. It is clearly understood that when epicenter distance increases, *z* displacements on the dam body surface diminish and less seismic effects occur on all nodal points on the dam body surface. Maximum *z* displacements for all cases are shown in Table 5.

In Fig. 12, 3D nonlinear seismic principal stress results are shown for 5 nodal points on the dam body surface. Total 5 various epicenter distances are considered in the seismic analyses and principal stress results for Case 1 are presented in Fig. 12(a). According to Fig. 12(a), maximum principal stress occurred on Point *D* and its numerical value is -21.1 MPa. It is clearly seen that maximum principal stress does not occur at bottom nodal point of the dam during the earthquake duration for CG dams. The greatest stresses occurred at slightly higher sections of the dam body base. When the other nodal points are examined, the maximum

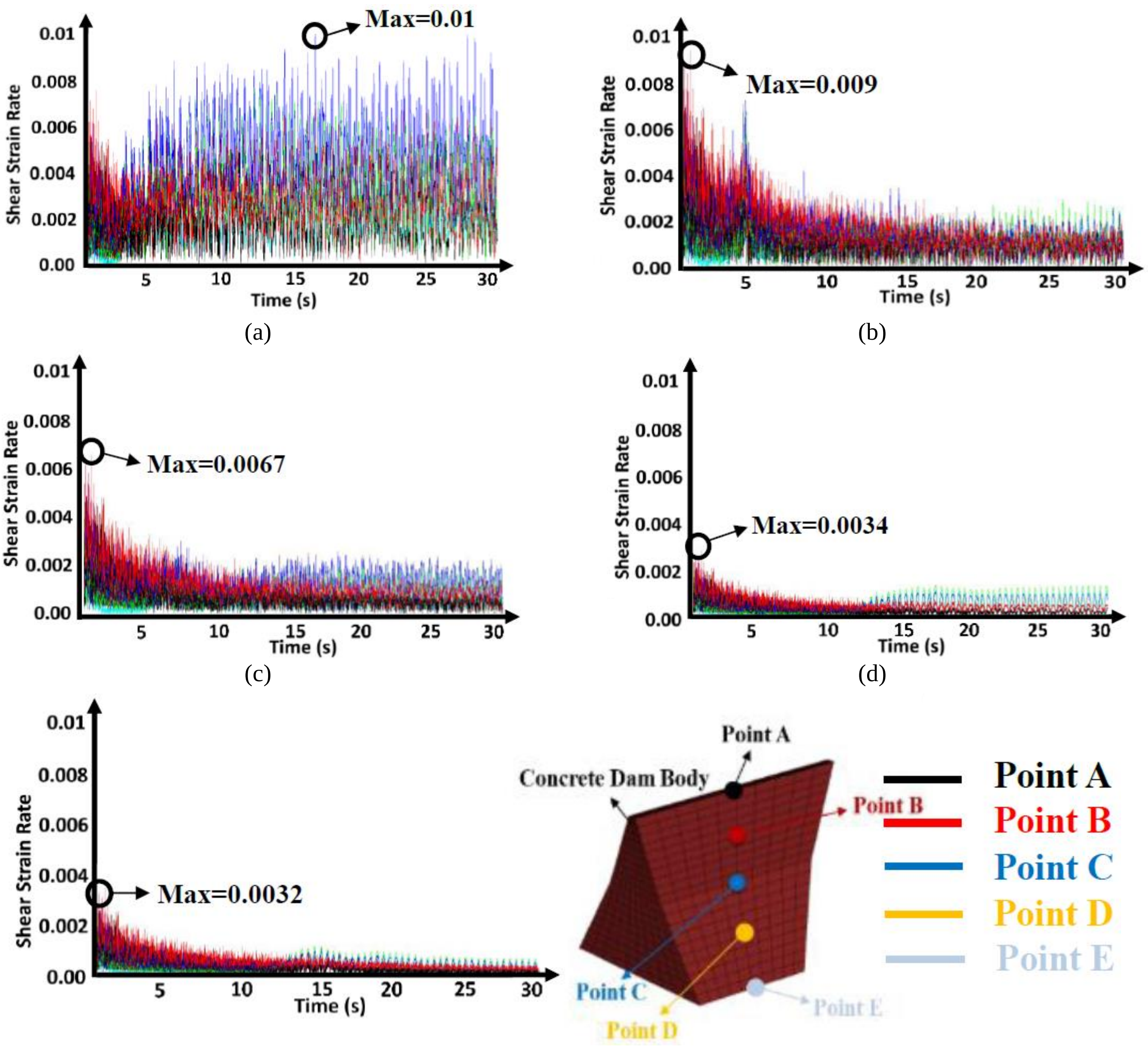

Fig. 13 Seismic shear strain failure (%) results for different epicenter distances of Loma Prieta earthquake: (a) Case 1 (epicenter distance: 5 km) (b) Case 2 (epicenter distance: 11 km) (c) Case 3 (epicenter distance: 24 km) (d) Case 4 (epicenter distance: 85 km) (e) Case 5 (epicenter distance: 93 km)

stresses occurred on Points *C*, *E*, *B* and *A*, respectively. Minimum stress is obtained on Point A (crest point). In Fig. 12(b), principal stress values are shown for Case 2. According to Fig. 12(b), maximum principal stress occurred on Point D and its numerical value is -15.1 MPa. In addition, minimum stress is observed on Point A. As compared Case 1 and Case 2, it is clearly seen the effects of epicenter distance on the 3D principal stress behavior of CG dams. When epicenter distance of earthquake increases, principal stress on the dam body surface obviously diminishes. Moreover, maximum principal stresses for other nodal points occurred on Points E, C, B, A, respectively. In Fig. 12(c), principal stress results are presented for Case 3. According to Fig. 12c, maximum stress is -12.4 MPa and it occurred on Point D. Moreover, minimum principal stress is observed on Point A (crest point). Maximum principal stress occurred at first seconds of the earthquake and less stress

Table 6 Maximum principal stresses for all cases

	Case 1	Case 2	Case 3	Case 4	Case 5
Max. Stress (MPa)	-21.1	-15.1	-12.4	-7.9	-5.6

results are obtained for Case 3 as compared with Case 2. In addition, principal stress results for Case 4 are shown in Fig. 12(d). Maximum principal stress occurred on Point D and its numerical value is -7.9 MPa. Minimum stress occurred on Point B. During first 10 seconds, there are no significant principal stress values on the dam body surface. According to Fig. 12(e), maximum principal stress is observed on Point D and its numerical value is -5.6 MPa. Moreover, no significant stresses did not occur on the dam body surface during first 13 seconds of the earthquake. It is clearly seen from these numerical results that nonlinear maximum principal stresses on the dam body surface obviously

Table 7 Maximum shear strain failures for all cases

	Case 1	Case 2	Case 3	Case 4	Case 5
Max. Failure (%)	0.01	0.009	0.0067	0.0034	0.0032

diminished from Case 1 to Case 5. In addition, maximum principal stresses for all cases are shown in Table 6. In Fig. 13, seismic shear strain failure behavior of Boyabat CG dam is examined considering 5 various ground motion distances. Generally, it is clearly seen from numerical results that maximum shear strain failure on the dam body surface is observed in Case 1 and minimum failure is obtained in Case 5. Moreover, it is obviously observed that maximum shear strain failure occurred on Point C (middle nodal point) for all epicenter distances. This result is very important to evaluate the crack and failure behavior of CG dam body. According to Fig. 13(a), shear strain failure behavior of the dam is investigated for Case 1. Maximum failure (%0.01) is observed on Point C and minimum failure occurred on Point A (crest point). This result clearly shows that if an earthquake occurs at dam site, concrete cracks will firstly start from middle section of the dam body surface. Moreover, shear strain failure results for Case 2 are presented in Fig. 13(b). According to Fig. 13(b), maximum shear strain failures are observed on Point B and its numerical value is %0.009. When compared Case 1 and Case 2, it is clearly seen that more shear strain failures are observed for Case 1. In Fig. 13(c), shear failure results are shown for Case 3. Maximum shear failure is %0.0067 and it is observed on Point B. In addition, minimum shear strain is obtained on crest point. Less shear strain failures are observed for Case 3 as compared with Cases 1 and 2. According to Fig. 13(d), maximum shear strain is obtained on Point B for Case 4 and its numerical value is %0.0034. For all nodal points, no significant shear failures are observed at last sections of the earthquake. Finally, shear failure behavior of Boyabat dam is shown for Case 5 in Fig. 13(e).

According to Fig. 13(e), maximum shear strain rate is %0.0032 and it occurred on Point B. As seen from these numerical results, when distance of epicenter to the dam increases, maximum shear strain failure clearly diminishes. This result proposes the effects of epicenter distance on 3D nonlinear shear strain behavior of CG dams. Moreover, Maximum shear strain failures for all cases are presented in Table 7.

7. Conclusions

In this paper, three dimensional (3D) nonlinear earthquake behavior of Boyabat concrete gravity (CG) dam is investigated under various epicenter distances of 1989 Loma Prieta earthquake. These ground motions are defined to 3D finite difference model using special fish functions and nonlinear seismic analyses of Boyabat CG dam body is assessed as below;

- In this study, it is strongly proposed that each epicenter distance has important seismic effects on the earthquake behavior of CG dams. Because of this reason, CG dams should not be randomly built. Furthermore, it is obviously revealed that as distance of epicenter to the dam increases, displacements on the dam body surface clearly diminish.
- For all epicenter distances, maximum displacements are observed on the crest point of the dam. According to seismic results, maximum *x* and *y* displacements on the dam body surface are obtained as +19.7 cm and +17.1 cm for 5 km epicenter distance. On the other hand, maximum *z* displacement on the dam body surface is -22.3 cm for the same epicenter distance. It is obviously seen that these maximum displacements are very significant for CG dam body due to these displacements might give rise to important engineering problems (e.g., cracks in the concrete body of the dam). Additionally, minimum displacements on the dam body surface occurred for 93 km epicenter distance.
- According to numerical analysis results, it is observed that the displacements occurring on the dam body surface greatly changed when epicenter distance is between 5 km and 24 km. On the other hand, from 24 km to 95 km, it is not observed that there are major changes in these displacements.
- At the end of the analyses results, the greatest stresses occurred at middle sections of the dam body base (Point *D*). When the other nodal points are observed, it is seen that the maximum stresses occurred on Points *C*, *E*, *B* and *A*, respectively. Furthermore, nonlinear maximum principal stresses on the dam body surface obviously diminished from 5 km epicenter distance to 93 km epicenter distance.
- Generally, it is clearly seen from seismic analyses that maximum shear strain failure on the dam body surface is observed in Case 1 (epicenter center: 5 km) and its numerical failure value is %0.01. On the other hand, minimum failure is obtained in Case 5 (epicenter center: 93 km). Moreover, it is obviously observed that maximum shear strain failure occurred on middle section of the dam body surface for all epicenter distances. This result clearly shows that if an earthquake occurs at dam site, concrete cracks will firstly start from the middle section of the dam body surface. Because of this reason, it is suggested that special designs and protections must be applied for this section of the dam.

References

Akköse, M., Şimşek, E. (2010), "Non-linear seismic response of concrete gravity dams to near-fault ground motions including dam water-sediment-foundation interaction", *Appl. Math. Model.*, **34**(11), 3685-3700. https://doi.org/10.1016/j.apm.2010.03.019.

Akpinar, U., Binici, B., Arici, Y. (2014), "Earthquake stresses and effective damping in concrete gravity dams", *Earthq. Struct.*, **6**(3). http://dx.doi.org/10.12989/eas.2014.6.3.251.

Chen, D.H., Du C.B. (2011), "Application of strength reduction method to dynamic anti-sliding stability analysis of high gravity dam with complex dam foundation", *Water Sci. Eng.*, **4**(2), 212-224. https://doi.org/10.3882/j.issn.1674-2370.2011.02.009.

Chen, D.H., Yang, Z.H., Wang, M., Xie, J.H. (2019), "Seismic performance and failure modes of the Jin'anqiao concrete gravity dam based on incremental dynamic analysis", *Eng. Failure Anal.*, **100**, 227-244. https://doi.org/10.1016/j.engfailanal.2019.02.018.

Chopra, A K. (1966), "Hydrodynamic pressures on dams during earthquakes", *Berkeley, Structures and Materials*, Report no. 66-2A. University of California Berkeley, California, U.S.A.

Fanelli, M. (1992), "Dynamic characterization of Talvacchia dam: Experimental activities, numerical modelling and monitoring", *Bergamo, Italy: Istituto sperimentale modelli e strutture*, ISMES publication, Serie: 334.

Fenves, G., Chopra, A. K. (1984), "EAGD-84: a computer program for earthquake analysis of concrete gravity dams", *Berkeley, Earthquake Engineering Research Centre.* Report no. UCB/EERC-84/11. University of California Berkeley, California, U.S.A.

Fok, K.L., Chopra, A. K. (1985), "Earthquake analysis and response of concrete arch dams", *Earthquake Engineering Research Centre*. Report no. UCB/EERC-85/07. University of California Berkeley, California, U.S.A.

Haciefendioglu, K., Bayraktar, A., Turker, T. (2010), "Seismic response of concrete gravity dam-ice covered reservoir-foundation interaction systems", *Struct. Eng. Mech.*, **36**(4).

Hai-tao, W., Jiayu, S., Feng, W., Zhiqiang, A., Tianyun, L. (2019), "Experimental study on elastic-plastic seismic response analysis of concrete gravity dam with strain rate effect", *Soil Dyn. Earthq. Eng.*, **116**, 563-569. https://doi.org/10.1016/j.soildyn.2018.09.020.

Hall, J. F. (1988), "The dynamic and earthquake behaviour of concrete dams: review of experimental behaviour and observational evidence", *Soil Dyn. Earthq. Eng*, **7**(2), 58–121. https://doi.org/10.1016/S0267-7261(88)80001-0.

Hariri-Ardebili, M.A., Seyed-Kolbadi, S.M., Mirzabozorg, H. (2013), "A smeared crack model for seismic failure analysis of concrete gravity dams considering fracture energy effects", *Struct. Eng. Mech.*, **4**8(1). DOI: 10.12989/sem.2013.48.1.017. https://doi.org/10.12989/sem.2010.36.4.499.

Itasca Consulting Group, Inc. FLAC version 5 user manual. Minneapolis, USA: Itasca Consulting Group, Inc.: 2002.

Lei, X. (2010), "Possible roles of the Zipingpu reservoir in triggering the 2008 Wenchuan earthquake", J. *Asian Earth Sci.*, **40**(4), 844–854. https://doi.org/10.1016/j.jseaes.2010.05.004.

Lotfi, V., Samii, A. (2012), "Dynamic analysis of concrete gravity dam-reservoir systems by wavenumber approach in the frequency domain", *Earthq. Struct.*, **3**(3). DOI: 10.12989/eas.2012.3.3_4.533.

Lysmer, J., Kuhlemeyer, RL., (1969), "Finite Dynamic Model for Infinite Media", *J. Eng. Mech.*, **95**(EM4), 859-877.

Mirzabozorg, H., Kianoush, R., Varmazyari, M. (2010), "Nonlinear behavior of concrete gravity dams and effect of input spatially variation", *Struct. Eng. Mech.*, **35**(3). http://dx.doi.org/10.12989/sem.2010.35.3.365.

Oudni, N., Bouafia, Y. (2015), "Response of concrete gravity dam by damage model under seismic excitation", *Eng. Failure Anal.*, **58**, 417-428. https://doi.org/10.1016/j.engfailanal.2015.08.020.

Poul, M.K., Zerva, A. (2018), "Nonlinear dynamic response of concrete gravity dams considering the deconvolution process", *Soil Dyn. Earthq. Eng.*, **109**, 324-338. https://doi.org/10.1016/j.soildyn.2018.03.025.

Seed, H.B., Idriss, I.M. (1970), "Soil moduli and damping factors for dynamic response analyses", *Technical Report EERRC-70-10*, University of California, Berkeley, U.S.A.

Sevim, B. (2018), "Geometrical dimensions effects on the seismic response of concrete gravity dams", *Advan. Concrete Constr.*, **6**(3), 269-283. https://doi.org/10.12989/acc.2018.6.3.269.

Wang, G., Wang, Y., Lu, W., Yan, P., Zhou, W., Chen, M. (2017), "Damage demand assessment of mainshock-damaged concrete gravity dams subjected to aftershocks", *Soil Dyn. Earthq. Eng.*, **98**, 141-154. https://doi.org/10.1016/j.soildyn.2017.03.034.

Wang, G., Wang, Y., Lu, W., Yu, M., Wang, C. (2017), "Deterministic 3D seismic damage analysis of Guandi concrete gravity dam: A case study", *Eng. Struct.*, **148**, 263-276. https://doi.org/10.1016/j.engstruct.2017.06.060.

Westergaard, H.M. (1933), "Water pressures on dams during earthquakes", *Am. Soc. Civ. Eng. Trans*., **98**(2), 418-433.

Yazdani, Y., Alembagheri, M. (2017), "Seismic vulnerability of gravity dams in near-fault areas", *Soil Dyn. Earthq. Eng.*, **102**, 15-24. https://doi.org/10.1016/j.soildyn.2017.08.020.

Zhang, S., Wang, G. (2013), "Effects of near-fault and far-fault ground motions on nonlinear dynamic response and seismic damage of concrete gravity dams", *Soil Dyn. Earthq. Eng.*, **53**, 217-229. https://doi.org/10.1016/j.soildyn.2013.07.014.

Zhu, H.H., Yin, J.H., Dong, J.H., Zhang, L. (2010), "Physical modelling of sliding failure of concrete gravity dam under overloading condition", *Geomech. Eng.*, **2**(2). https://10.12989/gae.2010.2.2.089.

CC